

Article

Copper Nanoparticles Confined in a Silica Nanochannel Film for the Electrochemical Detection of Nitrate Ions in Water Samples

Dewang Li ^{1,2}, Shuai Xu ³, Haiyan Jin ^{1,2}, Jinqing Wang ⁴  and Fei Yan ^{3,*} 

¹ Donghai Laboratory, Zhoushan 316021, China; dwli@sio.org.cn (D.L.); jinhaiyan@sio.org.cn (H.J.)

² Key Laboratory of Marine Ecosystem Dynamics, Second Institute of Oceanography, Ministry of Natural Resources, Hangzhou 310012, China

³ School of Chemistry and Chemical Engineering, Zhejiang Sci-Tech University, Hangzhou 310018, China; 202120104178@mails.zstu.edu.cn

⁴ College of Metrology and Measurement Engineering, China Jiliang University, Hangzhou 310018, China; jqwang@cjlu.edu.cn

* Correspondence: yanfei@zstu.edu.cn

Abstract: The nitrate ion (NO_3^-) is a typical pollutant in environmental samples, posing a threat to the aquatic ecosystem and human health. Therefore, rapid and accurate detection of NO_3^- is crucial for both the aquatic sciences and government regulations. Here we report the fabrication of an amino-functionalized, vertically ordered mesoporous silica film (NH_2 -VMSF) confining localized copper nanoparticles (CuNPs) for the electrochemical detection of NO_3^- . NH_2 -VMSF-carrying amino groups possess an ordered perpendicular nanochannel structure and ultrasmall nanopores, enabling the confined growth of CuNPs through the electrodeposition method. The resulting CuNPs/ NH_2 -VMSF-modified indium tin oxide (ITO) electrode (CuNPs/ NH_2 -VMSF/ITO) combines the electrocatalytic reduction ability of CuNPs and the electrostatic attraction capacity of NH_2 -VMSF towards NO_3^- . Thus, it is a rapid and sensitive electrochemical method for the determination of NO_3^- with a wide linear detection range of 5.0–1000 μM and a low detection limit of 2.3 μM . Direct electrochemical detection of NO_3^- in water samples (tap water, lake water, seawater, and rainwater) with acceptable recoveries ranging from 97.8% to 109% was performed, demonstrating that the proposed CuNPs/ NH_2 -VMSF/ITO sensor has excellent reproducibility, regeneration, and anti-interference abilities.

Keywords: copper nanoparticles; silica nanochannel film; nitrate ions; electrochemical sensor; water samples



Citation: Li, D.; Xu, S.; Jin, H.; Wang, J.; Yan, F. Copper Nanoparticles Confined in a Silica Nanochannel Film for the Electrochemical Detection of Nitrate Ions in Water Samples. *Molecules* **2023**, *28*, 7515. <https://doi.org/10.3390/molecules28227515>

Academic Editors: Ewa Szyrka and Magdalena Slowik-Borowiec

Received: 9 October 2023

Revised: 5 November 2023

Accepted: 7 November 2023

Published: 10 November 2023



Copyright: © 2023 by the authors. Licensee MDPI, Basel, Switzerland. This article is an open access article distributed under the terms and conditions of the Creative Commons Attribution (CC BY) license (<https://creativecommons.org/licenses/by/4.0/>).

1. Introduction

In the past few decades, nitrate ion (NO_3^-) pollution in water environments has become a serious global environmental issue [1]. The wide-spread use of nitrogen fertilizers and fossil fuels dramatically increases food production and the human population. However, the excess nitrogen on land and in the air has adverse effects on aquatic ecosystems and human health. Excessive use of nitrogen-containing fertilizers in agriculture and livestock farming, along with the uncontrolled discharge of wastewater into the groundwater, can result in the contamination of multiple aquatic environments [2]. Emissions of industrial gases are also a source of nitrate pollution, which can form nitric acid and further acidify lakes and streams through atmospheric deposition [3]. Increased nitrogen flowing into estuarine and nearshore waters contributes to the eutrophication of coastal waters. This phenomenon leads to a rise in the occurrence of harmful algal blooms, coastal hypoxia, and the degradation of habitats [4]. The ultimate oxidation product of inorganic nitrogen, NO_3^- , accounts for more than 65% of the dissolved nitrogen in seawater. Its status and fate

are crucial to the marine biogeochemical cycles of carbon [5], whose coupling regulates the climate on Earth [6]. As for human health, high levels of NO_3^- intake in the human body induce methemoglobinemia, colorectal cancer, thyroid disease, and neural tube defects [7]. For these reasons, the World Health Organization, the Food and Agriculture Organization, and governments have all set strict limits on NO_3^- in drinking water [8,9]. Therefore, simple and sensitive methods for the quantitative analysis of NO_3^- in aquatic environments are urgently needed for the aquatic science community and governments.

Various methods for NO_3^- determination include the visible spectrophotometric method using color reagents [10], direct ultraviolet spectrophotometry [11], fluorescence [12], chemiluminescence [13], electrochemical sensors [14], high-performance liquid chromatography [15], and ion chromatography [16]. Electrochemical sensing has gained widespread popularity because it generally offers a fast response time, high sensitivity, space-saving designs, and cost-efficiency [17–19]. However, electrochemical process of NO_3^- at the common electrodes is rather slow and produces high overpotentials. To overcome this issue, researchers have focused on the exploitation of various nanomaterials, such as metal nanoparticles [20], carbon nanotubes/fibers [21], and graphene-based materials [22]. Copper nanoparticles (CuNPs) have been reported as an effective electrocatalytic material for NO_3^- and nitrite (NO_2^-) reduction and have been combined with other carbonaceous materials for the sensitive determination of NO_3^- and NO_2^- [23–25].

Recently, mesoporous materials integrated with various functional nanomaterials have shown great potential in the fields of adsorption, catalysis, and sensing [26–31]. Vertically ordered mesoporous silica film (VMSF, also referred to as silica nanochannel film) has opened a vast range of potential opportunities for the electrochemical analysis of complicated real samples in recent decades [32–34]. VMSFs consisting of vertically oriented, open nanochannels attached to the electrode ensure the accessible transport of analytes or probes to the VMSF/electrode interface [35–37]. In addition, VMSFs have the electrostatic accumulation capacity for the target analyte due to the silanol groups on the walls and tiny nanochannels; at the same time, the insulating silica membrane can impede the ingress of interfering substances to the underlying electrode surface via charge, size, and lipophilicity interactions, showing good sensitivity, reproducibility, and long-term stability in real media analysis [38–40]. To enhance analytical sensitivity, electrocatalytic and/or conductive nanomaterials, such as metal nanoparticles [41], graphene quantum dots [42], and graphene nanosheets [43–46], have been incorporated into the inner space or bottom of VMSFs. Metal nanoparticles (e.g., gold and platinum) have been synthesized within the tiny nanochannels of VMSFs for the construction of attractive electrochemical sensors. To the best of our knowledge, CuNPs confined in the silica nanochannels of VMSFs have not yet been reported.

In this study, we synthesized electrodeposited CuNPs using an amino-functionalized, vertically ordered mesoporous silica film (NH_2 -VMSF) as a hard template. Their electrochemical performance with regard to NO_3^- quantification in environmental water samples has been examined. Many uniform, tiny NH_2 -VMSF nanochannels favor the localized, stable growth of CuNPs, avoiding the use of any protective agent. The resulting CuNPs/ NH_2 -VMSF-modified indium tin oxide (ITO) electrode, referred to as CuNPs/ NH_2 -VMSF/ITO, exhibits superior analytical performance with respect to NO_3^- due to the electrocatalytic properties of the CuNPs and the electrostatic accumulation ability of NH_2 -VMSF. Moreover, the CuNPs/ NH_2 -VMSF/ITO sensor we developed exhibits excellent reproducibility, regeneration, and anti-interference capabilities, which have been successfully employed to accurately measure the concentration of NO_3^- in diverse environmental water samples, including tap water, lake water, seawater, and rainwater.

2. Results and Discussion

2.1. Characterizations of NH_2 -VMSF/ITO and CuNPs/ NH_2 -VMSF/ITO Electrodes

Figure 1 shows the schematic illustration of the preparation of a CuNPs/ NH_2 -VMSF/ITO sensor and the electrochemical reduction detection of NO_3^- , which is divided into the

following three sections: First, a binary film consisting of surfactant micelles (SM) and VMSF-bearing amino groups, abbreviated as SM@NH₂-VMSF/ITO, was grown onto the patterned ITO electrode using the traditional electrochemical-assisted self-assembly (EASA) method [47,48] (Figure 1a). EASA combines electrochemical deposition and self-assembly techniques, inducing the self-assembly of SMs on the ITO electrode surface and the sol-gel process of the silane precursors within several seconds. SMs consisting of CTAB micelles are physically confined within the ultrasmall nanochannel space of the NH₂-VMSF and can be excluded by simple solvent extraction [49]. The addition of (3-aminopropyl) triethoxysilane into the precursor solution can result in the silica nanochannels carrying amino groups [50]. The NH₂-VMSF/ITO with an ultrasmall, open nanochannel array provided a confined nanospace for the stable synthesis of CuNPs with no protective agents. CuNPs were grown into the nanochannels of the NH₂-VMSF using a controllable electrodeposition method to form the CuNPs/NH₂-VMSF/ITO (Figure 1b), and their fabrication conditions (electrodeposition time) were also optimized. Not only could the CuNPs/NH₂-VMSF/ITO enrich NO₃[−] through electrostatic interaction between the amino groups of the NH₂-VMSF and NO₃[−], but it also exhibited the capacity to electrocatalytically reduce NO₃[−] via CuNPs. NO₃[−] could enter into the nanochannels of the NH₂-VMSF and be electrochemically reduced to NO₂[−] in an acidic environment (Figure 1c), ultimately giving rise to the reductive peak and enabling the quantitative determination of NO₃[−]. The anti-fouling properties of NH₂-VMSF make the proposed CuNPs/NH₂-VMSF/ITO sensor suitable for direct analysis of NO₃[−] in practical water samples.

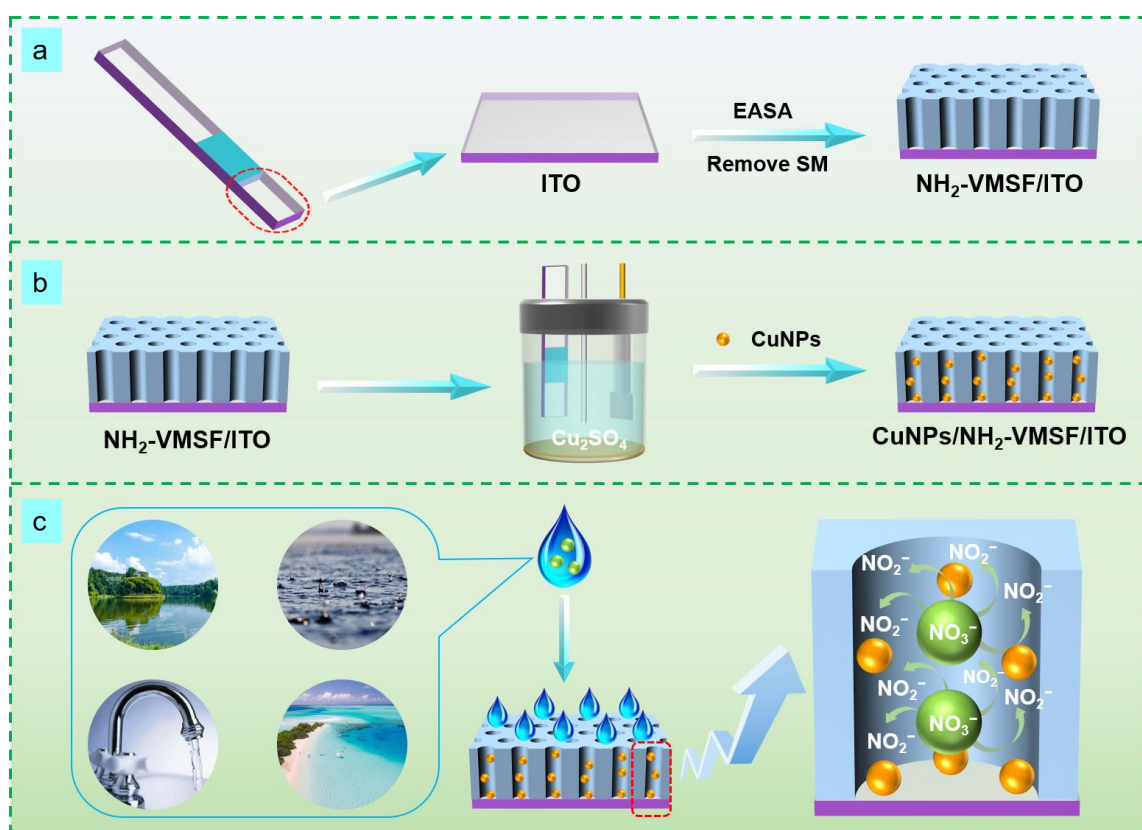


Figure 1. Schematic diagram of the preparation of an NH₂-VMSF/ITO sensor (a) and a CuNPs/NH₂-VMSF/ITO sensor (b) and the electrochemical reduction detection of NO₃[−] (c).

An NH₂-VMSF layer grown on the ITO surface was investigated by transmission electron microscopy (TEM). As shown in Figure 2a, the NH₂-VMSF, which was prepared using the electrochemically assisted self-assembly method with a high level of ordering, has a great deal of uniformly and hexagonally distributed nanopores (top-view TEM).

The average pore diameter of the NH₂-VMSF was in the range of 2–3 nm. Nanochannels oriented orthogonally to the NH₂-VMSF surface were parallel to each other with a length of 92 nm (cross-sectional view SEM, Figure 2b). Modification of the NH₂-VMSF layer with the permselective properties of the ITO was able to give rise to distinct electrochemical responses towards charged probes compared to a bare ITO electrode. Figure 2c,d shows the cyclic voltammetry (CV) curves of bare ITO, NH₂-VMSF/ITO and SM@NH₂-VMSF/ITO electrodes in a buffer solution containing either 50 μM Fe(CN)₆^{3−} or 50 μM Ru(NH₃)₆³⁺. As can be seen, both Fe(CN)₆^{3−} and Ru(NH₃)₆³⁺ were able to generate a pair of reversible redox peaks on the bare ITO (black curve). When insulating the NH₂-VMSF with a SM inside the nanochannels, no Faradic current was measured at the SM@NH₂-VMSF/ITO electrode (blue curve), because the templated SM molecules blocked access of charged hydrophilic probes; this further indicates that intact the NH₂-VMSF homogeneously covers the whole ITO electrode surface. Effective exclusion of SMs from the nanochannels could be achieved using a HCl–ethanol solution to obtain the NH₂-VMSF/ITO with recovered electrode accessibility [51]. Amino groups on the NH₂-VMSF were exposed to the buffer solution and carried positive charges under the measured experimental conditions (pH = 7.0), leading to enhanced voltammetric currents for Fe(CN)₆^{3−} (anodic peak current, *I*_{ox}, 33.7 μA vs. 24.4 μA (bare ITO)), while decreasing signals for Ru(NH₃)₆³⁺ (*I*_{ox}, 33.7 μA vs. 24.4 μA (bare ITO)) at the NH₂-VMSF/ITO electrode. The values of the peak-to-peak separation obtained at the NH₂-VMSF/ITO electrode were slightly larger than those at the bare ITO, suggesting the transport of probes into the nanochannels of NH₂-VMSF is effective. This anion-selective permeability of the NH₂-VMSF/ITO is due to the protonation of amino groups on the channel walls of the NH₂-VMSF and to pronounced electrostatic interaction within the tiny space [52].

The surface appearance of the NH₂-VMSF before and after the confined growth of CuNPs for an electrodeposition time of 10 s and 15 s (abbreviated as CuNPs_{10s}/NH₂-VMSF/ITO and CuNPs_{15s}/NH₂-VMSF/ITO) was examined via scanning electron microscopy (SEM). As seen in Figure 3a–c, the CuNPs_{10s}/NH₂-VMSF/ITO gave rise to a smooth surface, which was similar to that of the NH₂-VMSF/ITO, suggesting that electrodeposited CuNPs were inside the tiny nanochannels of the NH₂-VMSF. However, numerous nanoparticles were observed at the surface of the CuNPs_{15s}/NH₂-VMSF/ITO (Figure 3c), which resulted from the formation of inhomogeneous, large CuNPs on the top surface of the NH₂-VMSF when the electrodeposition time for the CuNPs was extended to 15 s (Figure 3d). Therefore, longer electrodeposition time can lead to the extended growth of CuNPs from the nanochannel to the surface of the NH₂-VMSF/ITO. CuNPs on the surface of the NH₂-VMSF/ITO are unstable and easily fall off the electrode surface, while those inside the silica nanochannels exhibit high stability due to the confinement effect. Considering the stability issue of the fabricated electrode, 10s was selected as the optimal electrodeposition time to guarantee the growth of CuNPs inside the nanochannels. Figure 3e shows CV curves for the NH₂-VMSF/ITO and CuNPs/NH₂-VMSF/ITO electrodes in a 0.1 M KCl solution. By comparison, the CuNPs/NH₂-VMSF/ITO electrode exhibited the characteristic peaks of CuNPs, namely anodic peaks at −0.15 V and 0.10 V, corresponding to the oxidation of Cu(0) to Cu(I) and Cu(I) to Cu(II), and cathodic peaks at −0.09 V and −0.50 V, corresponding to the reduction of Cu(II) to Cu(I) and Cu(I) to Cu(0). Figure 3f shows the XPS spectrum of the CuNPs/NH₂-VMSF/ITO, and the inset shows a magnified view of the peak of Cu 2p, demonstrating the presence of CuNPs. All of these results confirm the successful confinement of CuNPs inside the nanochannels of the NH₂-VMSF via the electrodeposition procedure.

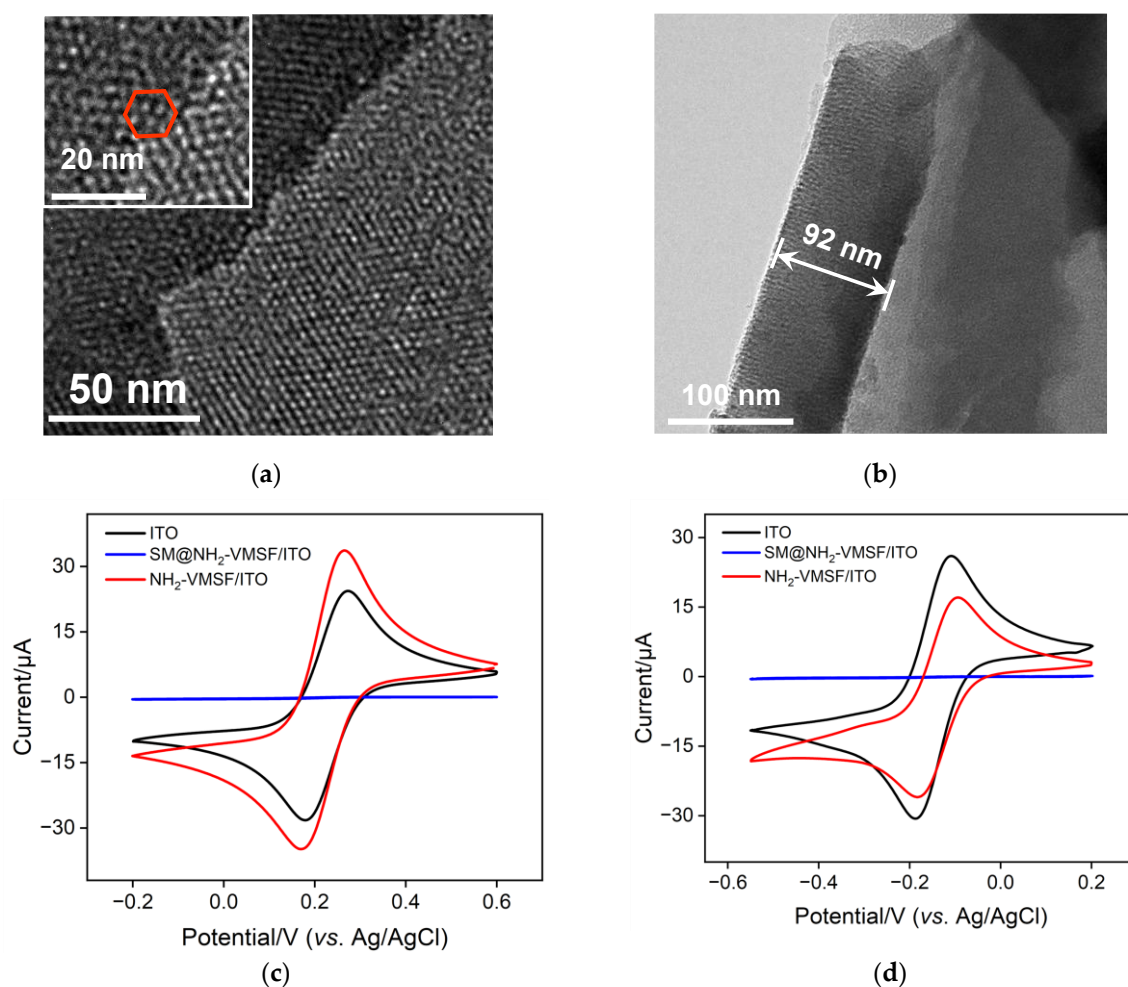


Figure 2. (a) Top-view and (b) cross-sectional TEM images of the NH₂-VMSF. The inset in (a) is the corresponding magnified image showing hexagonally distributed nanopores. CV responses of ITO (black), VMSF/ITO (red) and SM@VMSF/ITO (blue) to 50 μM Fe(CN)₆³⁻ (c) and 50 μM Ru(NH₃)₆³⁺ (d) at a scan rate of 50 mV/s. The supporting electrolytes for Fe(CN)₆³⁻ and Ru(NH₃)₆³⁺ are 0.05 M KHP.

2.2. Electrocatalytic Reduction of NO₃⁻ Using CuNPs/NH₂-VMSF/ITO

Figure 4a depicts the electrochemical reduction ability of the fabricated CuNPs/NH₂-VMSF/ITO electrode towards NO₃⁻. Upon the addition of 300 μM NO₃⁻ into a 0.1 M Na₂SO₄ (pH = 3.0) solution, an obvious cathodic peak was observed at the CuNPs/NH₂-VMSF/ITO electrode, which was attributed to the electrocatalytic reduction of NO₃⁻ at the fabricated electrode. Figure 4b compares the CV and DPV responses of the CuNPs/NH₂-VMSF/ITO, NH₂-VMSF/ITO and bare ITO electrodes towards 300 μM NO₃⁻ in a 0.1 M Na₂SO₄ (pH = 3.0) solution. As shown, no cathodic peak signal was observed at the bare ITO electrode and a weak signal was obtained at the NH₂-VMSF/ITO electrode due to the electrostatic interaction between the positively charged channel walls and the negatively charged NO₃⁻. After electrodeposition of CuNPs into the nanochannels, the CuNPs/NH₂-VMSF/ITO exhibited a significantly increased cathodic peak current for NO₃⁻, which was attributed to the excellent electrocatalytic ability of CuNPs and the porous nanostructure of the NH₂-VMSF for the growth of numerous CuNPs. Therefore, the inherent nanocatalytic properties of CuNPs and the electrostatic accumulation ability were combined to obtain a highly sensitive determination of NO₃⁻, showing superior analytical performance.

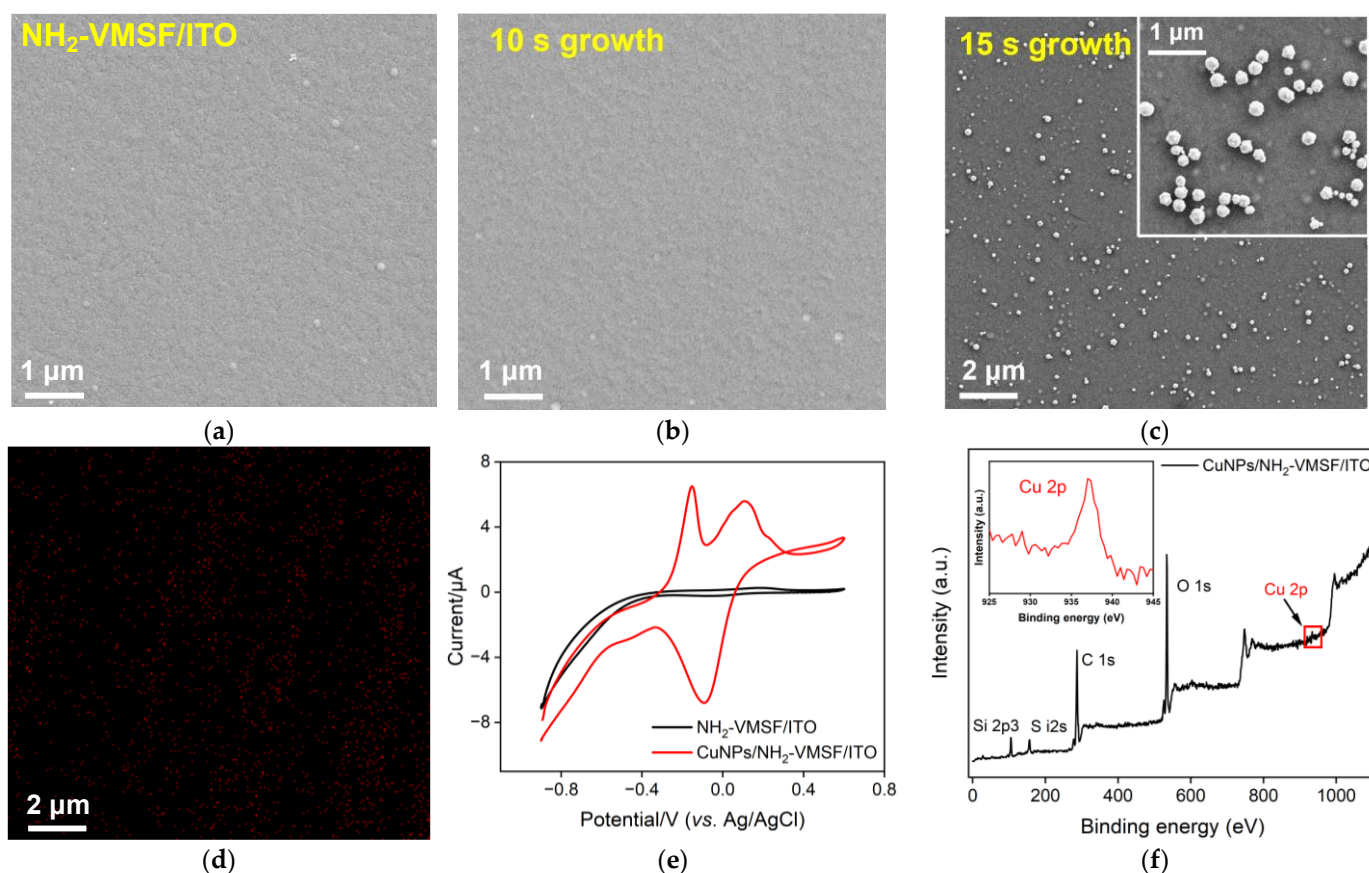


Figure 3. Top-view SEM images of the $\text{NH}_2\text{-VMSF/ITO}$ before (a) and after the confined growth of CuNPs for an electrodeposition time of 10 s (b) and 15 s (c). (d) The Cu element mapping image of the $\text{CuNPs/NH}_2\text{-VMSF/ITO}$ from Figure 2c. (e) CV curves of the $\text{NH}_2\text{-VMSF/ITO}$ and $\text{CuNPs/NH}_2\text{-VMSF/ITO}$ electrodes in a 0.1 M KCl solution. (f) XPS spectra of the $\text{CuNPs/NH}_2\text{-VMSF/ITO}$; the inset is a magnified view of the red box in the figure.

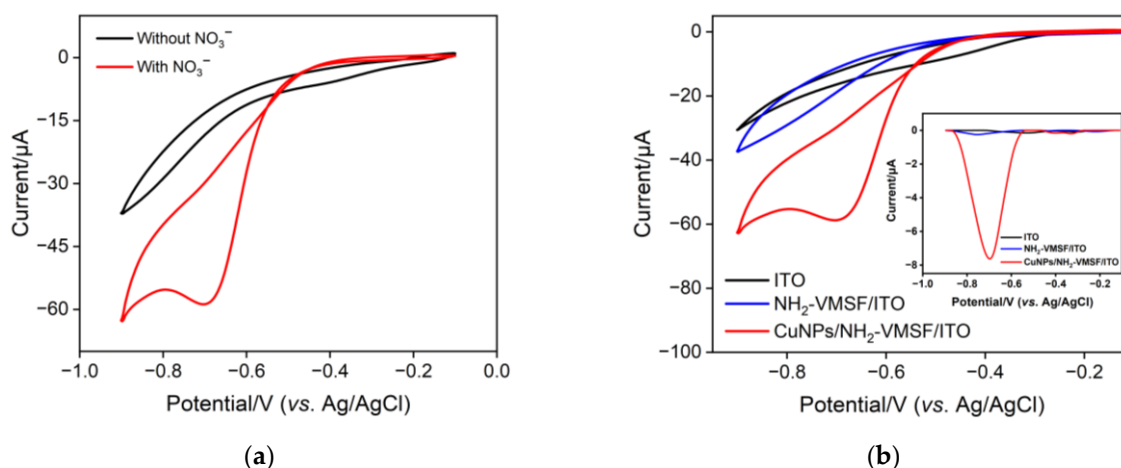


Figure 4. (a) CV curves of a fabricated $\text{CuNPs/NH}_2\text{-VMSF/ITO}$ electrode in 0.1 M Na_2SO_4 (pH = 3.0) in the absence and presence of $300 \mu\text{M NO}_3^-$. (b) CV responses of bare ITO, $\text{NH}_2\text{-VMSF/ITO}$, and $\text{CuNPs/NH}_2\text{-VMSF/ITO}$ electrodes towards $300 \mu\text{M NO}_3^-$ in 0.1 M Na_2SO_4 (pH = 3.0). The inset in (b) shows the corresponding DPV curves for $300 \mu\text{M NO}_3^-$.

The mechanism for the electrocatalytic reduction of NO_3^- on the $\text{CuNPs/NH}_2\text{-VMSF/ITO}$ electrode was investigated via CV and differential pulse voltammetry (DPV).

Figure 5a shows the CV curves of 300 μM NO_3^- in 0.1 M Na_2SO_4 (pH = 3.0) at the CuNPs/ NH_2 -VMSF/ITO under different scan rates. The cathodic peak current (I_{pc}) and cathodic peak (E_{pc}) of 300 μM NO_3^- at the CuNPs/ NH_2 -VMSF/ITO were extracted from Figure 5a and plotted as a function of scan rate (v) and natural logarithm ($\ln v$), respectively. As shown in Figure 5b, the I_{pc} was linearly proportional to the v within the range of 60 to 220 mV/s, suggesting a surface-controlled electrocatalytic reduction process of NO_3^- at the CuNPs/ NH_2 -VMSF/ITO. The relation between E_{pc} and $\ln v$ was linear as shown in Figure 5c and can be expressed as the following equation:

$$E_{\text{pc}} = -0.0243 \ln v - 0.6310 \quad (R^2 = 0.9903) \quad (1)$$

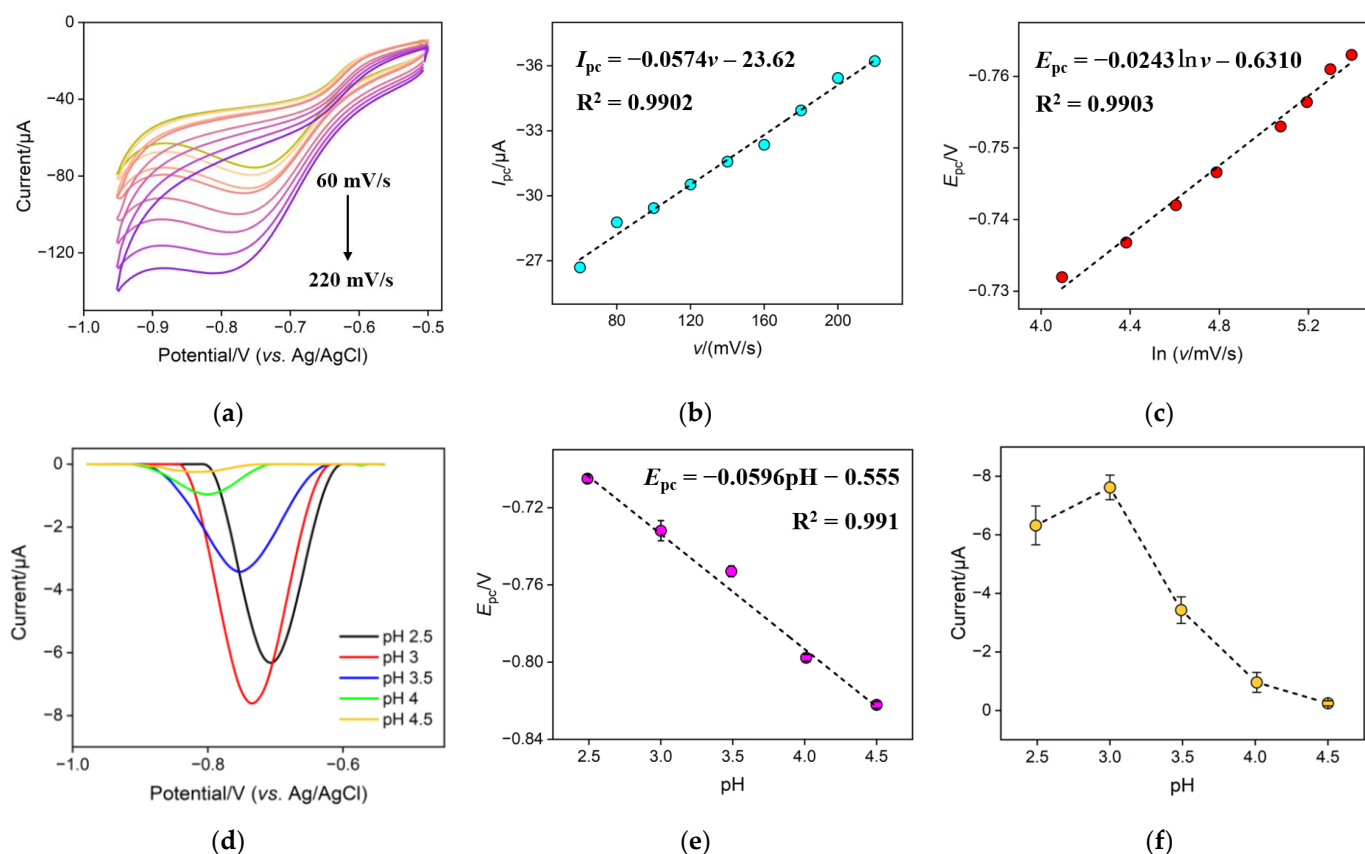


Figure 5. (a) CV curves for 300 μM NO_3^- in 0.1 M Na_2SO_4 (pH = 3.0) at the CuNPs/ NH_2 -VMSF/ITO under different scan rates (from top to bottom: 60, 80, 100, 120, 140, 160, 180, 200, and 220 mV/s). (b) The plot of the cathodic peak current (I_{pc}) obtained from (a) against scan rate (v). (c) The plot of the cathodic peak (E_{pc}) obtained from (a) against the natural logarithm of the scan rate ($\ln v$). (d) DPV responses of the CuNPs/ NH_2 -VMSF/ITO for 300 μM NO_3^- in 0.1 M Na_2SO_4 , adjusted to various pH values. The plots of the E_{pc} (e) and cathodic peak current (f) obtained from (d) against the pH value.

The Laviron equation was used as follows to describe the relationship between E_{pc} and $\ln v$:

$$E_{\text{pc}} = E'_0 + \left(\frac{RT}{\alpha nF} \right) \ln \left(\frac{RTK_s}{\alpha nF} \right) - \left(\frac{RT}{\alpha nF} \right) \ln v \quad (2)$$

where E'_0 , K_s , α , and n are the standard electrode potential, the standard heterogeneous rate constant, the transfer coefficient, and the number of electrons involved in the rate-determining step, respectively. Other symbols have their usual physical meanings: R , gas constant ($8.314 \text{ J mol}^{-1} \text{ K}^{-1}$); T , absolute temperature (298 K); F , Faraday constant ($96,485 \text{ C mol}^{-1}$).

The following can be deduced from Equations (1) and (2):

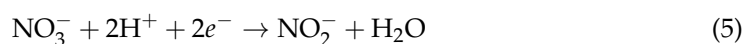
$$\left(\frac{RT}{\alpha nF}\right) = 0.0243 \quad (3)$$

According to Equation (3), the value of αn was calculated to be 1.05. Given a α of 0.5 in the completely irreversible electrochemical reaction, n was calculated to be 2.1, indicating that the reduction process of NO_3^- involves two electrons.

The slope of the fitting linear relationship between E_{pc} and pH could be used to determine the ratio of electrons and protons participating in the electrochemical reaction on the electrode surface. Figure 5d shows the DPV curves of the CuNPs/ NH_2 -VMSF/ITO electrode for 300 μM NO_3^- in 0.1 M Na_2SO_4 , adjusted to various pH values. As the curves demonstrate, E_{pc} became more negative as the pH increased. The good linear relationship shown in Figure 5e in the range of 2.5 to 4.5 can be expressed as follows:

$$E_{\text{pc}} = -0.0596\text{pH} - 0.555 \quad (R^2 = 0.991) \quad (4)$$

Given that $\frac{dE_{\text{pc}}}{\text{d pH}} = 2.303 \frac{mRT}{nF}$, where m is the number of protons and the other symbols are the same as above, the calculated m/n for the NO_3^- reduction process was 1.01, indicating equal involvement of protons and electrons in the electrochemical reduction of NO_3^- . Combining an n of 2 as obtained above, it could be inferred that the electrochemical reduction reaction of NO_3^- is a two-electron coupled, two-proton process, which can be shown as follows:



2.3. Influence of Experimental Conditions on Electrochemical Detection of NO_3^-

To obtain good analytical performance, the influence of the pH value of the Na_2SO_4 solution on the reduction of NO_3^- was investigated. Figure 5f shows the cathodic peak current for 300 μM NO_3^- in 0.1 M Na_2SO_4 at the CuNPs/ NH_2 -VMSF/ITO at different pH values. The cathodic peak current initially increased with increasing pH, reaching a maximum at pH 3, and then decreased as the pH continued to increase. When the pH was less than 3, a hydrogen evolution reaction occurred at a less negative potential in strongly acidic media, which could affect the reduction of NO_3^- . When the pH was greater than 3, a decrease in the cathodic peak current of NO_3^- was found. This is because the hydrogen ions participate in the electrochemical reduction reaction of NO_3^- to NO_2^- . An increase in pH made the chemical equilibrium (Equation (5)) shift to the left, leading to the decreased cathodic peak current. Therefore, pH 3 was selected as the optimum condition.

Optimizing the amount of CuNPs inside the nanochannels of the NH_2 -VMSF was crucial to the effective accumulation of NO_3^- for achieving the highest sensitivity. The electrodeposition time of CuNPs can be used for determining the amount of CuNPs inside the nanochannels, which was studied in Figure 6a. As shown here, when the electrodeposition time of the CuNPs increased from 0 s to 10 s, the electrochemical reduction signal of NO_3^- gradually improved, because having more CuNPs inside the nanochannels enhanced the electrocatalytic capacity for NO_3^- reduction. But further increasing the electrodeposition time causes excessive aggregation of CuNPs on the outer surface of the NH_2 -VMSF channels. Therefore, the optimal electrodeposition time for the growth of CuNPs was achieved at 10 s. The inner walls of the NH_2 -VMSF channels are rich in amino groups, which carry positive charges in acidic environments and exhibit electrostatic adsorption towards NO_3^- . When the CuNPs/ NH_2 -VMSF/ITO was magnetically stirred in a buffer solution containing 100 μM NO_3^- , the achieved cathodic peak current signal increased significantly from 0 to 6 min (Figure 6b), which was due to more NO_3^- having diffused to the underlying electrode surface through the nanochannels of the NH_2 -VMSF. After 6 min, the cathodic peak current of NO_3^- remained unchanged. Therefore, the accumulation time of 6 min was employed for the subsequent test.

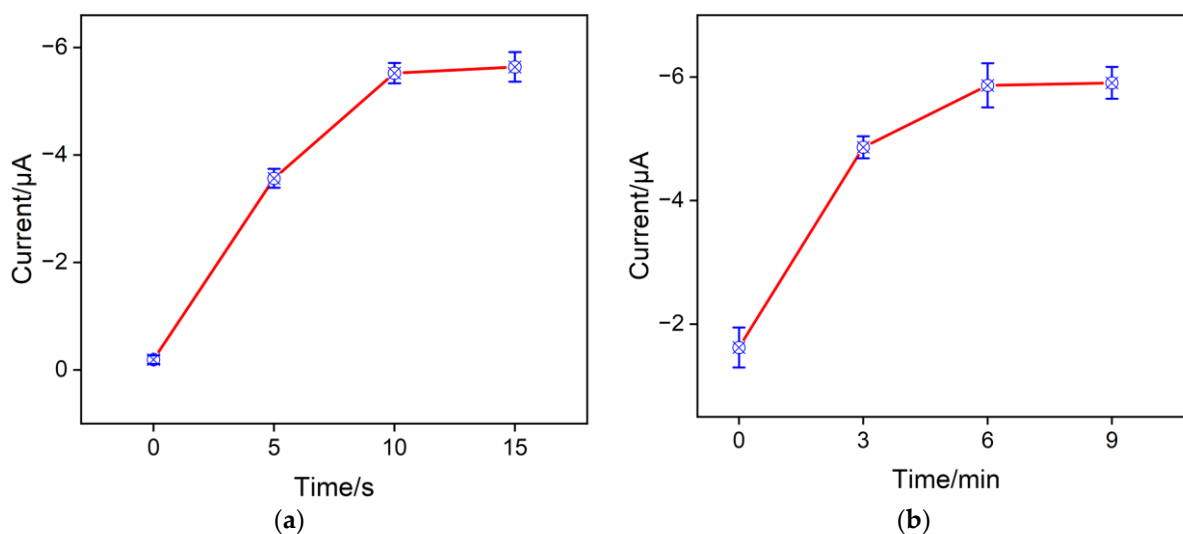


Figure 6. Effects of electrodeposition time (a) on the growth of CuNPs and of mechanical stirring time (b) for the preconcentration of NO₃⁻ on the electrochemical responses for 100 μM NO₃⁻ at the CuNPs/NH₂-VMSF/ITO in a Na₂SO₄ (0.1 M, pH = 3) solution.

2.4. Electroanalytical Performance of NO₃⁻ Using CuNPs/NH₂-VMSF/ITO

The differential pulse voltammetry (DPV) technique was used to determine different concentrations of NO₃⁻ in a 0.1 M Na₂SO₄ solution using the CuNPs/NH₂-VMSF/ITO electrode. Figure 7 shows the DPV signals and calibration curves of NO₃⁻ in the range of 5 μM⁻¹ mM. As presented, the cathodic peak current of NO₃⁻ tested at the CuNPs/NH₂-VMSF/ITO electrode grew linearly with concentration. The linear regression equation in the range of 5–100 μM can be expressed as $I (\mu\text{A}) = 0.051 C (\mu\text{M}) + 0.29$ ($R^2 = 0.996$), and the other linear regression equation in the range of 100–1000 μM as $I (\mu\text{A}) = 0.021 C (\mu\text{M}) + 3.77$ ($R^2 = 0.998$). The limit of detection (LOD) was estimated to be 2.3 μM at a signal-to-noise ratio of three using the formula of $\text{LOD} = 3\text{SD}/k$ (where SD and k are the standard deviation of the blank solution and the slope of the calibration curve, respectively). Note that the LOD value is far below the concentration limit (806 μM) for NO₃⁻ in the water quality standard specified by World Health Organization. Moreover, the proposed CuNPs/NH₂-VMSF/ITO has several advantages over other electrodes reported in the literature, such as a lower LOD, a wider dynamic linear range, and easy fabrication steps (Table 1).

2.5. Anti-Interference, Regeneration, Reproducibility, and Stability of CuNPs/NH₂-VMSF/ITO

The selectivity of the prepared CuNPs/NH₂-VMSF/ITO sensor for NO₃⁻ detection was evaluated in the presence of common interfering ions, such as 1 mM Na²⁺, K⁺, Ca²⁺, Mg²⁺, Na⁺, NO₂⁻, Cl⁻, Br⁻, SO₄²⁻, PO₄³⁻, and SO₃²⁻. As shown in Figure 8a, a ten-fold concentration of these interfering ions produced minimal interference for the determination of 100 μM NO₃⁻ at the CuNPs/NH₂-VMSF/ITO, indicating the good selectivity and anti-interference ability of the proposed sensor. To assess the electrode's regeneration capacity, the same CuNPs/NH₂-VMSF/ITO electrode was used to repeatedly measure 300 μM NO₃⁻; the used electrode was washed with a 0.1 M HCl–ethanol solution for 5 min prior to testing. As shown in Figure 8b, no significant decrease in the current signal was observed at our fabricated sensor after five-time elution, demonstrating the excellent regeneration ability of the sensor. Five batches of CuNPs/NH₂-VMSF/ITO electrodes were prepared under the same conditions and used to test 300 μM NO₃⁻ in order to examine the reproducibility of the electrode. The calculated relative standard deviation (RSD) of the measured results from the five electrodes was 1.8% (Figure 8c), confirming the high reproducibility of the CuNPs/NH₂-VMSF/ITO electrode. Additionally, the stability of the fabricated CuNPs/NH₂-VMSF/ITO electrode was studied by comparing the initial

cathodic peak current of NO_3^- with that obtained after five days in storage. The data shown in Figure 8d prove the good stability of CuNPs/ NH_2 -VMSF/ITO electrode under a nitrogen atmosphere compared with storage under an air atmosphere.

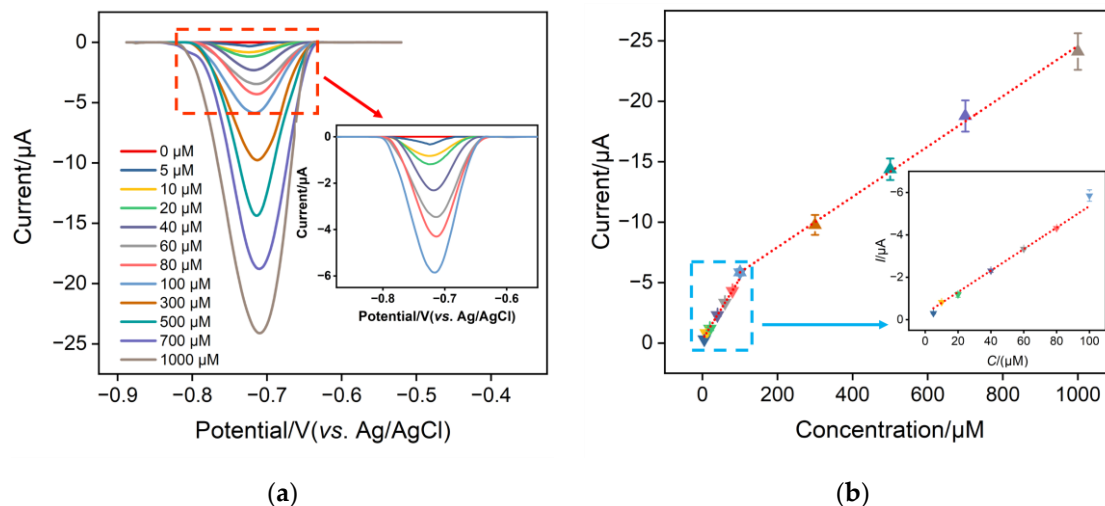


Figure 7. (a) DPV responses of the CuNPs/ NH_2 -VMSF/ITO to the successive addition of various concentrations of NO_3^- in a Na_2SO_4 (0.1 M, pH 3.0) solution. The concentrations of NO_3^- range from 5 μM to 1000 μM . (b) The cathodic peak current—concentration plot for the CuNPs/ NH_2 -VMSF/ITO electrode with the addition of various concentrations of NO_3^- in a Na_2SO_4 (0.1 M, pH 3.0) solution. Insets in (a,b) represent the corresponding amplified curves in the low concentration range, and the error bars in (b) represent the standard deviations of three measurements.

Table 1. Analytical results of several modified electrodes for the detection of NO_3^- .

Electrode	Detection Method	Linear Range (μM)	LOD (μM)	Real Sample	Ref.
Cu-NWs/copper tape	LSV	$10.0\text{--}1.5 \times 10^3$	9.1	river, rainwater and drinking	[53]
PEG-SH/SePs/AuNPs/PCE	DPV	$16.0\text{--}5 \times 10^3$	8.6	lake water	[54]
Cu@TiO ₂ -Nf/PAR/GCE	DPV	$5.0\text{--}7.5 \times 10^3$	2.1	river water and tap water	[55]
Cu/MWCNT/RGO/GCE	SWV	0.1×75	0.02	mineral water tap water and	[56]
Pt/Ag/ITO	CV	$266\text{--}4.4 \times 10^3$	134.0	simulated ground water	[57]
IIP-Cu-NPs/PANI/GCE	EIS	$1.0\text{--}1 \times 10^3$	31.0	mineral water	[58]
Cu-NWs/Cu wire	LSV	50.0–600	5.0	well water	[59]
CuNPs/ NH_2 -VMSF/ITO	DPV	$5.0\text{--}1 \times 10^3$	12.2	not shown	[59]
			2.3	tap water, pond water, seawater and rainwater	This work

Cu-NWs: copper nanowires. PEG-SH: poly(ethyleneglycol) methylether thiol. SePs: selenium particles. AuNPs: gold nanoparticles. PCE: paper carbon electrode. Nf: nafion. PAR: polyalazarin yellowe R. MWCNT: multiwall carbon nanotubes. RGO: reduced graphene oxide. IIP: ion-imprinted polymer. PANI: polyaniline.

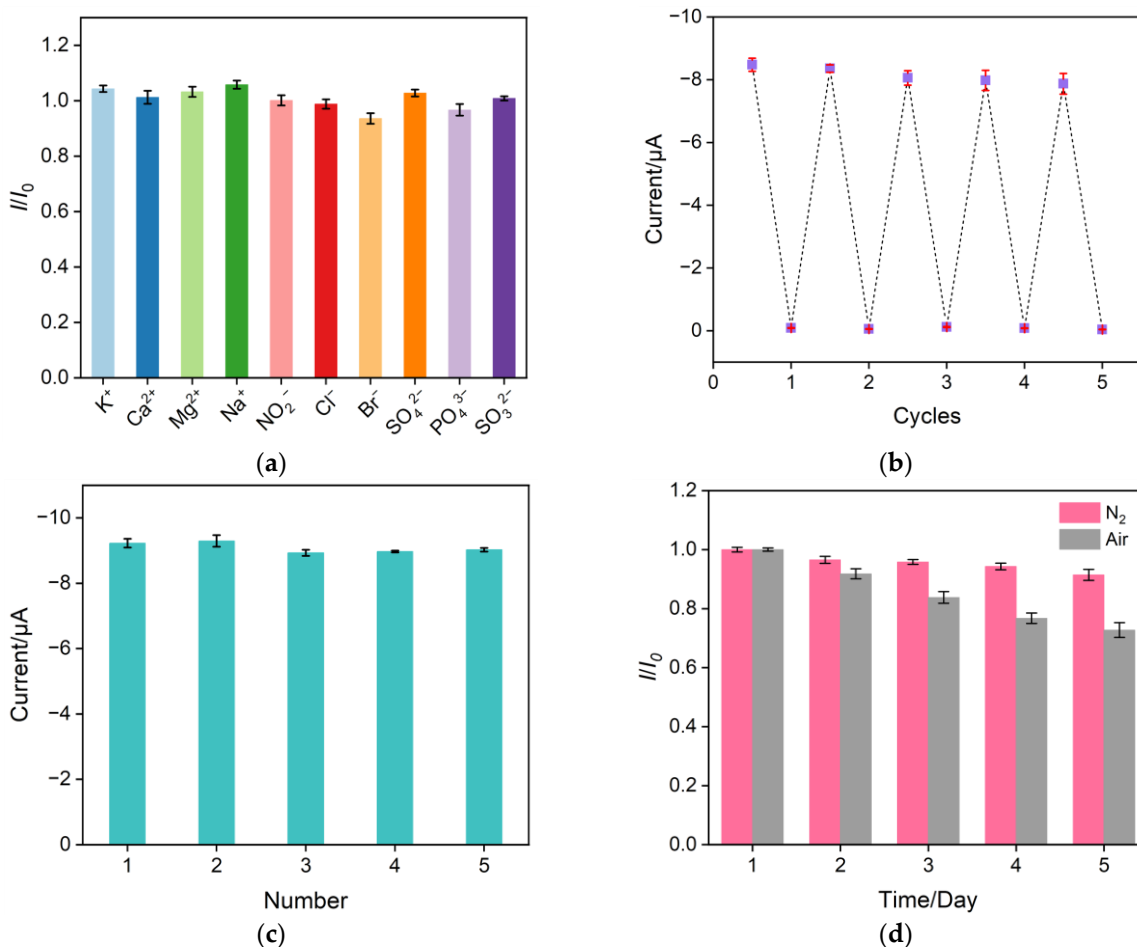


Figure 8. (a) Cathodic peak current ratio obtained at the developed CuNPs/ NH_2 -VMSF/ITO electrode for the detection of $100 \mu\text{M NO}_3^-$ before (I_0) and after (I) the addition of 1 mM of various interfering substances to a Na_2SO_4 solution (0.1 M pH = 3). (b) DPV signals of $300 \mu\text{M NO}_3^-$ measured repeatedly after multiple elutions of the CuNPs/ NH_2 -VMSF/ITO electrode. (c) DPV signals of $300 \mu\text{M NO}_3^-$ in a Na_2SO_4 solution (0.1 M pH = 3) measured using five different electrodes prepared in parallel. (d) DPV signals of the CuNPs/ NH_2 -VMSF/ITO electrodes for the detection of $300 \mu\text{M NO}_3^-$ in a 0.1 M Na_2SO_4 (pH = 3) solution after storage for different numbers of days in air and nitrogen atmospheres, respectively. The error bars represent the standard deviations of three measurements.

2.6. Direct Analysis of NO_3^- in Water Samples

According to the previous reports, NH_2 -VMSF serves as a good anti-fouling protective layer on the electrode surface and has been used to design many electrochemical sensors in rather complicated real samples [38]. Environmental water samples including tap water, rainwater, lake water, and seawater were selected to validate the practical applicability of our fabricated CuNPs/ NH_2 -VMSF/ITO electrode. The pH of these collected water samples was adjusted to 3 using sulfuric acid, and several known concentrations of NO_3^- were added. The CuNPs/ NH_2 -VMSF/ITO electrode was then used to analyze the above samples using the DPV technique. Table 2 shows the quantitative results for NO_3^- in water samples using the standard addition method. As shown, our proposed CuNPs/ NH_2 -VMSF/ITO electrode exhibited excellent recovery values ranging from 97.8% to 109%, demonstrating the good analytical performance of the developed sensor in real water samples.

Table 2. Quantification of NO_3^- in real samples using CuNPs/ NH_2 -VMSF/ITO electrode.

Sample	Added (μM)	Found (μM)	Recovery (%)	RSD (% , $n = 3$)
Tap Water	10.0	10.2	102	0.9
	100	103	103	1.9
	500	495	99.0	3.1
Pond Water	30.0	32.8	109	3.9
	100	97.8	97.8	3.4
	500	503	101	1.2
Rainwater	30.0	29.9	99.6	2.6
	100	100	100	1.6
	500	505	101	0.8
Seawater	30.0	30.9	103	2.3
	100	101	101	3.4
	500	518	104	1.3

3. Materials and Methods

3.1. Chemicals and Instrumentations

All analytical grade chemicals and reagents in this study were used as received without further purification. Ultrapure water was obtained from the Millipore Milli-Q system (18 M Ω cm). Tetraethoxysilane (TEOS), cetyltrimethylammonium bromide (CTAB), and (3-aminopropyl) triethoxysilane (APTES) were purchased from Sigma-Aldrich. Potassium ferricyanide ($\text{K}_3[\text{Fe}(\text{CN})_6]$), hexaammineruthenium (III) chloride ($[\text{Ru}(\text{NH}_3)_6\text{Cl}_3]$), and acetone were ordered from Shanghai Aladdin Biochemical Technology Co., Ltd. Sodium sulfate (Na_2SO_4), sodium sulfite (Na_2SO_3), sodium nitrite (NaNO_2), sodium phosphate (Na_3PO_4), sodium chloride (NaCl), potassium chloride (KCl), potassium bromide (KBr), potassium nitrate (KNO_3), and copper (II) sulfate pentahydrate ($\text{CuSO}_4 \cdot 5\text{H}_2\text{O}$) were bought from Shanghai Macklin Biochemical Technology Co., Ltd. (Shanghai, China) Indium tin oxide (ITO) conductive glass (surface resistivity < 17 Ω /square, thickness of 100 ± 20 nm) were purchased from Zhuhai Kaivo Optoelectronics Technology Co., Ltd. (Zhuhai, China) The ITO glass was sonicated with 1 M aqueous sodium hydroxide for two hours, followed by acetone, ethanol, and deionized water sonication for ten minutes each. Finally, the ITO glass was dried at 60 $^\circ\text{C}$ prior to use.

The shape and thickness of the NH_2 -VMSF were determined using transmission electron microscopy (TEM, HT7700, Hitachi, Japan) and scanning electron microscopy (SEM, SU8010, Hitachi, Japan) at accelerating voltages of 200 kV and 5 kV, respectively. A PHI5300 electron spectrometer (PE Ltd., Boston, MA, USA) was used to conduct an X-ray photoelectron spectroscopy (XPS) examination with 250 W, 14 kV Mg K radiation. Electrochemical impedance spectroscopy (EIS), cyclic voltammetry (CV), and differential pulse voltammetry (DPV) measurements were carried out using an Autolab electrochemical workstation (PGSTAT302N, Metrohm, Switzerland). Measurements of electrochemical reactions were performed using a conventional three-electrode system. A bare ITO or modified ITO ($0.5 \times 1 \text{ cm}^2$), an Ag/AgCl (saturated with KCl solution), and a platinum wire were selected as the working electrode, the reference electrode, and the counter electrode, respectively.

3.2. Preparation of the NH_2 -VMSF/ITO Electrode

The NH_2 -VMSF was grown on a conductive ITO electrode using the electrochemically assisted self-assembly (EASA) method [35]. A mixed solution composed of 20 mL ethanol, 20 mL 0.1 M NaNO_3 , 13.6 mM "TEOS + APTES" (9:1 molar ratio), and 4.35 mM CTAB were first prepared. After adjusting the pH to 3.0 with hydrochloric acid (HCl, 3 M), the precursor solution was stirred for 2.5 h at room temperature. A clean ITO ($0.5 \times 1 \text{ cm}^2$) was immersed into the precursor solution and electrodeposited at a constant current of -0.35 mA for 10 s. The resulting electrode was immediately removed from the growth solution, thoroughly

rinsed with ultrapure water, dried under a nitrogen atmosphere, and aged overnight at 120 °C. During the preparation process, a surfactant micelle (SM) consisting of CTAB served as a template and remained in the nanochannels of the NH₂-VMSF; this was given the designation SM@NH₂-VMSF/ITO. SMs can be easily eliminated by stirring in 50 mL of an ethanol solution containing 0.1 M hydrochloric acid for 5 min. The resulting electrode was designated as the NH₂-VMSF/ITO electrode.

3.3. Electrochemical Deposition of CuNPs

The electrochemical deposition of CuNPs into the NH₂-VMSF was modified slightly according to reference [56] as follows: 0.5 mmol CuSO₄·5H₂O was added to 50 mL of a 0.1 M sulfuric acid solution and sonicated for 5 min to obtain the electrodeposition solution. Then, the NH₂-VMSF/ITO/ITO electrode was placed in the above electrodeposition solution and was subjected to a constant potential of −0.6 V for 10 s using a platinum sheet as the counter electrode and Ag/AgCl as the reference electrode. Finally, the resulting electrode was rinsed with ultrapure water and blow-dried with nitrogen gas, yielding the CuNPs/NH₂-VMSF/ITO electrode.

3.4. Detection of NO₃[−]

Before the electrochemical test, the Na₂SO₄ solution (0.1 M and pH adjusted to 3.0 with sulfuric acid) was deoxygenated by bubbling nitrogen gas in the solution for 30 min. Various concentrations of NO₃[−] were added to the above solution and determined using the CuNPs/NH₂-VMSF/ITO electrode under a nitrogen atmosphere. The DPV parameters included a step potential of 0.005 V, a pulse amplitude of 0.05 V, an interpulse time of 0.2 s, and a pulse time of 0.05 s.

3.5. Actual Sample Testing

Tap water, rainwater, lake water, and seawater were selected as actual samples to verify the accuracy of the CuNPs/NH₂-VMSF/ITO sensor using the standard addition method. Tap water, lake water, and rainwater in the samples were sourced locally (Hangzhou, China), and seawater produced in Qingdao (Shandong, China) was purchased from Taobao. The pH of these environmental water samples was adjusted to 3 using sulfuric acid (0.1 M) without dilution. Different concentrations of NO₃[−] were added to the water samples and then determined using the CuNPs/NH₂-VMSF/ITO sensor.

4. Conclusions

A simple and highly sensitive NO₃[−] electrochemical sensor was developed based on an NH₂-VMSF and CuNPs confined in the nanochannels. Physical confinement of CuNPs was achieved via a controllable one-step electrodeposition procedure. The immobilization of the CuNPs in the tiny nanochannels endows the electrode with the electrocatalytic capacity for reducing NO₃[−] and conducting highly sensitive NO₃[−] measurements. Not only can the NH₂-VMSF serve as a hard template for the stable growth of CuNPs, but it can also provide the electrostatic accumulation capacity for the target NO₃[−]. The detection limit for this kind of CuNPs/NH₂-VMSF/ITO sensor is as low as 2.3 μM with a linear range extending from 5.0 μM to 1 mM for NO₃[−] determinations. Furthermore, direct analysis of NO₃[−] concentrations in various environmental samples using our proposed sensor was evaluated, revealing acceptable accuracy and great promise for fast NO₃[−] monitoring in samples of polluted water such as sewage.

Author Contributions: Investigation, D.L. and H.J.; data curation, D.L., S.X. and J.W.; writing—original draft preparation, D.L.; validation, H.J. and J.W.; writing—review and editing, conceptualization and supervision, F.Y.; project administration, D.L. and F.Y. All authors have read and agreed to the published version of the manuscript.

Funding: This research was jointly funded by Science Foundation of Donghai Laboratory (Grant no. DH-2022KF0201), the project of the Donghai Laboratory (Grant no. DH-2022ZY0006), Scientific Research Fund of the Second Institute of Oceanography, MNR (QNYJ2203), Zhejiang Provincial Natural Science Foundation of China (LY21B050003), and the Fundamental Research Funds of Zhejiang Sci-Tech University (22062310-Y).

Institutional Review Board Statement: Not applicable.

Informed Consent Statement: Not applicable.

Data Availability Statement: The data presented in this study are available on request from the corresponding author.

Conflicts of Interest: The authors declare no conflict of interest.

References

1. Camargo, J.A.; Alonso, Á. Ecological and toxicological effects of inorganic nitrogen pollution in aquatic ecosystems: A global assessment. *Environ. Int.* **2006**, *32*, 831–849. [[CrossRef](#)] [[PubMed](#)]
2. Zhao, B.; Sun, Z.; Liu, Y. An overview of in-situ remediation for nitrate in groundwater. *Sci. Total Environ.* **2022**, *804*, 149981. [[CrossRef](#)] [[PubMed](#)]
3. Brimblecombe, P.; Stedman, D.H. Historical evidence for a dramatic increase in the nitrate component of acid rain. *Nature* **1982**, *298*, 460–462. [[CrossRef](#)]
4. Howarth, R.W. Coastal nitrogen pollution: A review of sources and trends globally and regionally. *Harmful Algae* **2008**, *8*, 14–20. [[CrossRef](#)]
5. Gruber, N.; Galloway, J.N. An Earth-system perspective of the global nitrogen cycle. *Nature* **2008**, *451*, 293–296. [[CrossRef](#)] [[PubMed](#)]
6. Sigman, D.M.; Boyle, E.A. Glacial/interglacial variations in atmospheric carbon dioxide. *Nature* **2000**, *407*, 859–869. [[CrossRef](#)]
7. Ward, M.H.; Jones, R.R.; Brender, J.D.; De Kok, T.M.; Weyer, P.J.; Nolan, B.T.; Villanueva, C.M.; Van Breda, S.G. Drinking water nitrate and human health: An updated review. *Int. J. Environ. Res. Public Health* **2018**, *15*, 1557. [[CrossRef](#)]
8. Abascal, E.; Gómez-Coma, L.; Ortiz, I.; Ortiz, A. Global diagnosis of nitrate pollution in groundwater and review of removal technologies. *Sci. Total Environ.* **2022**, *810*, 152233. [[CrossRef](#)]
9. Yu, G.; Wang, J.; Liu, L.; Li, Y.; Zhang, Y.; Wang, S. The analysis of groundwater nitrate pollution and health risk assessment in rural areas of Yantai, China. *BMC Public Health* **2020**, *20*, 437. [[CrossRef](#)]
10. Hansen, H.P.; Koroleff, F. Determination of nutrients. In *Methods Seawater Analysis, 3rd*; Grasshoff, K., Kremling, K., Ehrhardt, M., Eds.; Wiley: Weinheim, Germany, 1999; pp. 159–228.
11. Johnson, K.S.; Coletti, L.J. In situ ultraviolet spectrophotometry for high resolution and long-term monitoring of nitrate, bromide and bisulfide in the ocean. *Deep. Sea Res. Part I Oceanogr. Res. Pap.* **2002**, *49*, 1291–1305. [[CrossRef](#)]
12. Strianese, M.; Milione, S.; Bertolasi, V.; Pellicchia, C. Iron and manganese pyridoxal-based complexes as fluorescent probes for nitrite and nitrate anions in aqueous solution. *Inorg. Chem.* **2013**, *52*, 11778–11786. [[CrossRef](#)] [[PubMed](#)]
13. Kodamatani, H.; Kubo, S.; Takeuchi, A.; Kanzaki, R.; Tomiyasu, T. Sensitive detection of nitrite and nitrate in seawater by 222 nm UV-irradiated photochemical conversion to peroxynitrite and ion chromatography-luminol chemiluminescence system. *Environ. Sci. Technol.* **2023**, *57*, 5924–5933. [[CrossRef](#)] [[PubMed](#)]
14. Kaminskaya, O.V.; Zakharova, E.A.; Slepchenko, G.B. Simultaneous voltammetric determination of nitrites and nitrates in waters. *J. Anal. Chem.* **2004**, *59*, 1091–1096. [[CrossRef](#)]
15. Khan, M.R.; Wabaidur, S.M.; Alothman, Z.A.; Busquets, R.; Naushad, M. Method for the fast determination of bromate, nitrate and nitrite by ultra performance liquid chromatography–mass spectrometry and their monitoring in Saudi Arabian drinking water with chemometric data treatment. *Talanta* **2016**, *152*, 513–520. [[CrossRef](#)] [[PubMed](#)]
16. Hern, J.A.; Rutherford, G.K.; Vanloon, G.W. Determination of chloride, nitrate, sulphate and total sulphur in environmental samples by single-column ion chromatography. *Talanta* **1983**, *30*, 677–682. [[CrossRef](#)] [[PubMed](#)]
17. Tan, J.F.; Anastasi, A.; Chandra, S. Electrochemical detection of nitrate, nitrite and ammonium for on-site water quality monitoring. *Curr. Opin. Electrochem.* **2022**, *32*, 100926. [[CrossRef](#)]
18. Gong, J.; Tang, H.; Wang, M.; Lin, X.; Wang, K.; Liu, J. Novel three-dimensional graphene nanomesh prepared by facile electro-etching for improved electroanalytical performance for small biomolecules. *Mater. Des.* **2022**, *215*, 110506. [[CrossRef](#)]
19. Liu, Q.; Zhong, H.; Chen, M.; Zhao, C.; Liu, Y.; Xi, F.; Luo, T. Functional nanostructure-loaded three-dimensional graphene foam as a non-enzymatic electrochemical sensor for reagentless glucose detection. *RSC Adv.* **2020**, *10*, 33739–33746. [[CrossRef](#)]
20. Fox, C.M.; Breslin, C.B. Electrochemical formation of silver nanoparticles and their applications in the reduction and detection of nitrates at neutral pH. *J. Appl. Electrochem.* **2020**, *50*, 125–138. [[CrossRef](#)]
21. Pan, D.; Lu, W.; Wu, S.; Zhang, H.; Qin, W. In situ spontaneous redox synthesis of carbon nanotubes/copper oxide nanocomposites and their preliminary application in electrocatalytic reduction of nitrate. *Mater. Lett.* **2012**, *89*, 333–335. [[CrossRef](#)]
22. Marlinda, A.R.; An'amt, M.N.; Yusoff, N.; Sagadevan, S.; Wahab, Y.A.; Johan, M.R. Recent progress in nitrates and nitrites sensor with graphene-based nanocomposites as electrocatalysts. *Trends Environ. Anal. Chem.* **2022**, *34*, e00162. [[CrossRef](#)]

23. Parveen, S.; Pathak, A.; Gupta, B.D. Fiber optic SPR nanosensor based on synergistic effects of CNT/Cu-nanoparticles composite for ultratrace sensing of nitrate. *Sens. Actuators B Chem.* **2017**, *246*, 910–919. [[CrossRef](#)]
24. Ferlazzo, A.; Bressi, V.; Espro, C.; Iannazzo, D.; Piperopoulos, E.; Neri, G. Electrochemical determination of nitrites and sulfites by using waste-derived nanobiochar. *J. Electroanal. Chem.* **2023**, *928*, 117071. [[CrossRef](#)]
25. Saha, P.; Akter, R.; Shaheen Shah, S.; Mahfoz, W.; Aziz, M.A.; Saleh Ahammad, A.J. Gold nanomaterials and their composites as electrochemical sensing platforms for nitrite detection. *Chem.-Asian J.* **2022**, *17*, e202200823. [[CrossRef](#)] [[PubMed](#)]
26. Zhao, J.; Duan, W.; Liu, X.; Xi, F.; Wu, J. Microneedle patch integrated with porous silicon confined dual nanozymes for synergistic and hyperthermia-enhanced nanocatalytic ferroptosis treatment of melanoma. *Adv. Funct. Mater.* **2023**, *2023*, 2308183. [[CrossRef](#)]
27. Duan, W.; Jin, Y.; Cui, Y.; Xi, F.; Liu, X.; Wo, F.; Wu, J. A co-delivery platform for synergistic promotion of angiogenesis based on biodegradable, therapeutic and self-reporting luminescent porous silicon microparticles. *Biomaterials* **2021**, *272*, 120772. [[CrossRef](#)]
28. Cui, Y.; Duan, W.; Jin, Y.; Wo, F.; Xi, F.; Wu, J. Ratiometric fluorescent nanohybrid for noninvasive and visual monitoring of sweat glucose. *ACS Sens.* **2020**, *5*, 2096–2105. [[CrossRef](#)]
29. Xu, S.; Zhang, S.; Li, Y.; Liu, J. Facile synthesis of iron and nitrogen Co-doped carbon dot nanozyme as highly efficient peroxidase mimics for visualized detection of metabolites. *Molecules* **2023**, *28*, 6064. [[CrossRef](#)]
30. He, J.; Li, Z.; Zhao, R.; Lu, Y.; Shi, L.; Liu, J.; Dong, X.; Xi, F. Aqueous synthesis of amphiphilic graphene quantum dots and their application as surfactants for preparing of fluorescent polymer microspheres. *Colloid Surf. A* **2019**, *563*, 77–83. [[CrossRef](#)]
31. Huang, Y.; Ding, Z.; Li, Y.; Xi, F.; Liu, J. Magnetic nanozyme based on loading nitrogen-doped carbon dots on mesoporous Fe₃O₄ nanoparticles for the colorimetric detection of glucose. *Molecules* **2023**, *28*, 4573. [[CrossRef](#)]
32. Walcarius, A. Electroinduced surfactant self-assembly driven to vertical growth of oriented mesoporous films. *Acc. Chem. Res.* **2021**, *54*, 3563–3575. [[CrossRef](#)] [[PubMed](#)]
33. Yan, Z.; Zhang, S.; Liu, J.; Xing, J. Homogeneous electrochemical aptamer sensor based on two-dimensional nanocomposite probe and nanochannel modified electrode for sensitive detection of carcinoembryonic antigen. *Molecules* **2023**, *28*, 5186. [[CrossRef](#)] [[PubMed](#)]
34. Lv, N.; Qiu, X.; Han, Q.; Xi, F.; Wang, Y.; Chen, J. Anti-biofouling electrochemical sensor based on the binary nanocomposite of silica nanochannel array and graphene for doxorubicin detection in human serum and urine samples. *Molecules* **2022**, *27*, 8640. [[CrossRef](#)] [[PubMed](#)]
35. Gong, J.; Zhang, T.; Luo, T.; Luo, X.; Yan, F.; Tang, W.; Liu, J. Bipolar silica nanochannel array confined electrochemiluminescence for ultrasensitive detection of SARS-CoV-2 antibody. *Biosens. Bioelectron.* **2022**, *215*, 114563. [[CrossRef](#)] [[PubMed](#)]
36. Yan, L.; Zhang, C.; Xi, F. Disposable amperometric label-free immunosensor on chitosan-graphene-modified patterned ITO electrodes for prostate specific antigen. *Molecules* **2022**, *27*, 5895. [[CrossRef](#)] [[PubMed](#)]
37. Huang, J.; Zhang, T.; Zheng, Y.; Liu, J. Dual-mode sensing platform for cancer antigen 15-3 determination based on a silica nanochannel array using electrochemiluminescence and electrochemistry. *Biosensors* **2023**, *13*, 317. [[CrossRef](#)]
38. Zhou, P.; Yao, L.; Chen, K.; Su, B. Silica nanochannel membranes for electrochemical analysis and molecular sieving: A comprehensive review. *Crit. Rev. Anal. Chem.* **2019**, *50*, 424–444. [[CrossRef](#)]
39. Wang, K.; Yang, L.; Huang, H.; Lv, N.; Liu, J.; Liu, Y. Nanochannel array on electrochemically polarized screen printed carbon electrode for rapid and sensitive electrochemical determination of clozapine in human whole blood. *Molecules* **2022**, *27*, 2739. [[CrossRef](#)]
40. Ma, K.; Yang, L.; Liu, J.; Liu, J. Electrochemical sensor nanoarchitectonics for sensitive detection of uric acid in human whole blood based on screen-printed carbon electrode equipped with vertically-ordered mesoporous silica-nanochannel film. *Nanomaterials* **2022**, *12*, 1157. [[CrossRef](#)]
41. Huang, L.; Su, R.; Xi, F. Sensitive detection of noradrenaline in human whole blood based on Au nanoparticles embedded vertically-ordered silica nanochannels modified pre-activated glassy carbon electrodes. *Front. Chem.* **2023**, *11*, 1126213. [[CrossRef](#)]
42. Zhang, C.; Zhou, X.; Yan, F.; Lin, J. N-doped graphene quantum dots confined within silica nanochannels for enhanced electrochemical detection of doxorubicin. *Molecules* **2023**, *28*, 6443. [[CrossRef](#)]
43. Zhu, X.; Xuan, L.; Gong, J.; Liu, J.; Wang, X.; Xi, F.; Chen, J. Three-dimensional macroscopic graphene supported vertically-ordered mesoporous silica-nanochannel film for direct and ultrasensitive detection of uric acid in serum. *Talanta* **2022**, *238*, 123027. [[CrossRef](#)] [[PubMed](#)]
44. Zhou, H.; Ding, Y.; Su, R.; Lu, D.; Tang, H.; Xi, F. Silica nanochannel array film supported by β -cyclodextrin-functionalized graphene modified gold film electrode for sensitive and direct electroanalysis of acetaminophen. *Front. Chem.* **2022**, *9*, 812086. [[CrossRef](#)]
45. Zheng, W.; Su, R.; Lin, X.; Liu, J. Nanochannel array modified three-dimensional graphene electrode for sensitive electrochemical detection of 2,4,6-trichlorophenol and prochloraz. *Front. Chem.* **2022**, *10*, 954802. [[CrossRef](#)]
46. Deng, X.; Lin, X.; Zhou, H.; Liu, J.; Tang, H. Equipment of vertically-ordered mesoporous silica film on electrochemically pretreated three-dimensional graphene electrodes for sensitive detection of methidazine in urine. *Nanomaterials* **2023**, *13*, 239. [[CrossRef](#)] [[PubMed](#)]
47. Walcarius, A.; Sibottier, E.; Etienne, M.; Ghanbaja, J. Electrochemically assisted self-assembly of mesoporous silica thin films. *Nat. Mater.* **2007**, *6*, 602–608. [[CrossRef](#)] [[PubMed](#)]
48. Chen, D.; Luo, X.; Xi, F. Probe-integrated electrochemical immunosensor based on electrostatic nanocage array for reagentless and sensitive detection of tumor biomarker. *Front. Chem.* **2023**, *11*, 1121450. [[CrossRef](#)]

49. Ma, N.; Luo, X.; Wu, W.; Liu, J. Fabrication of a disposable electrochemical immunosensor based on nanochannel array modified electrodes and gated electrochemical signals for sensitive determination of C-reactive protein. *Nanomaterials* **2022**, *12*, 3981. [[CrossRef](#)]
50. Zhou, X.; Han, Q.; Zhou, J.; Liu, C.; Liu, J. Reagentless electrochemical detection of tumor biomarker based on stable confinement of electrochemical probe in bipolar silica nanochannel film. *Nanomaterials* **2023**, *13*, 1645. [[CrossRef](#)]
51. Su, R.; Tang, H.; Xi, F. Sensitive electrochemical detection of p-nitrophenol by pre-activated glassy carbon electrode integrated with silica nanochannel array film. *Front. Chem.* **2022**, *10*, 954748. [[CrossRef](#)]
52. Luo, X.; Zhang, T.; Tang, H.; Liu, J. Novel electrochemical and electrochemiluminescence dual-modality sensing platform for sensitive determination of antimicrobial peptides based on probe encapsulated liposome and nanochannel array electrode. *Front. Nutr.* **2022**, *9*, 962736. [[CrossRef](#)] [[PubMed](#)]
53. Patella, B.; Russo, R.R.; O’Riordan, A.; Aiello, G.; Sunseri, C.; Inguanta, R. Copper nanowire array as highly selective electrochemical sensor of nitrate ions in water. *Talanta* **2021**, *221*, 121643. [[CrossRef](#)] [[PubMed](#)]
54. Bui, M.-P.N.; Brockgreitens, J.; Ahmed, S.; Abbas, A. Dual detection of nitrate and mercury in water using disposable electrochemical sensors. *Biosens. Bioelectron.* **2016**, *85*, 280–286. [[CrossRef](#)] [[PubMed](#)]
55. Amini, N.; Maleki, A.; Maleki, P. Electrochemical detection of nitrate ions via reduction of NO²⁻ and oxidation of NO reactions based on Cu@TiO₂ core-shell/nafion/polyalizarin immobilized electrode. *Mater. Chem. Phys.* **2021**, *264*, 124384. [[CrossRef](#)]
56. Bagheri, H.; Hajian, A.; Rezaei, M.; Shirzadmehr, A. Composite of Cu metal nanoparticles-multiwall carbon nanotubes-reduced graphene oxide as a novel and high performance platform of the electrochemical sensor for simultaneous determination of nitrite and nitrate. *J. Hazard. Mater.* **2017**, *324*, 762–772. [[CrossRef](#)]
57. Wang, J.; Diao, P. Simultaneous detection of ammonia and nitrate using a modified electrode with two regions. *Microchem. J.* **2020**, *154*, 104649. [[CrossRef](#)]
58. Essousi, H.; Barhoumi, H.; Bibani, M.; Ktari, N.; Wendler, F.; Al-Hamry, A.; Kanoun, O. Ion-imprinted electrochemical sensor based on copper nanoparticles-polyaniline matrix for nitrate detection. *J. Sens.* **2019**, *2019*, 4257125. [[CrossRef](#)]
59. Wu, Y.; Gao, M.; Li, S.; Ren, Y.; Qin, G. Copper wires with seamless 1D nanostructures: Preparation and electrochemical sensing performance. *Mater. Lett.* **2018**, *211*, 247–249. [[CrossRef](#)]

Disclaimer/Publisher’s Note: The statements, opinions and data contained in all publications are solely those of the individual author(s) and contributor(s) and not of MDPI and/or the editor(s). MDPI and/or the editor(s) disclaim responsibility for any injury to people or property resulting from any ideas, methods, instructions or products referred to in the content.